J. Fluid Mech. (1990), *vol.* 219, *pp.* 215–239
Printed in Great Britain

Temperature and velocity field regimes of convective motions in a rotating plane fluid layer

By B. M. BOUBNOV AND G. S. GOLITSYN
Institute of Atmospheric Physics of the USSR Academy of Sciences, 109017 Moscow, USSR

(Received 15 November 1988 and in revised form 14 March 1990)

The paper is a continuation of work published in Boubnov & Golitsyn (1986). We present new measurements of the temperature and velocity field patterns and their statistical characteristics. This allows us to classify regimes of convection in a plane rotating horizontal fluid layer in terms of Rayleigh and Taylor numbers. Within the irregular regimes geostrophic convection is found for which the Rossby number is much less than unity.

In the regular regimes the mean temperature profiles are linear with height in the bulk of the fluid, the gradient being dependent mainly on rotation rate Ω and fluid depth h. These together with some dimensional arguments lead to the heat transfer relationship $Nu \propto Ra^3 Ta^{-2}$ between Nusselt, Rayleigh and Taylor numbers. Experimental results by Rossby (1969) and theoretical work by Chan (1974) and Riahi (1977) suggested this dependence. The dependence on $\omega\tau$ of the temperature power spectrum normalized by the variance was found to be universal at higher frequencies for all irregular convective motions, where τ is the timescale of the thermal boundary layer for cases with a small influence of rotation and with τ about three times larger (in numerical coefficient) for geostrophic convection. For irregular geostrophic regimes it is found that the temperature variance depends on rotation rate and heat flux, and is inversely proportional to the buoyancy parameter.

Horizontal and vertical components of the velocity fields were measured for regular as well as irregular regimes, confirming, especially for geostrophic convection, the theoretical results by Golitsyn (1980). In conclusion some geophysical applications are briefly mentioned.

1. Introduction

The history of convection studies in rotating fluids starting from the works by Chandrasekhar (1953, 1961) and Nakagawa & Frenzen (1955) is described by Boubnov & Golitsyn (1986, hereinafter referred to as Paper 1). For convection in a plane horizontal fluid layer with depth h rotating around the vertical axis with a constant angular velocity Ω the basic determining parameters are the non-dimensional numbers of Rayleigh, Taylor and Prandtl:

$$Ra_f = \frac{\alpha g f h^4}{\rho c_p k^2 \nu}, \quad Ta = \frac{4\Omega^2 h^4}{\nu^2}, \quad Pr = \frac{\nu}{k}, \tag{1.1}$$

where α, k, ν are respectively the coefficients of the thermal expansion, thermodiffusivity and kinematic viscosity of the fluid, c_p is its specific heat content, ρ is the density, g is the acceleration due to gravity, and f is the heat flux coming into

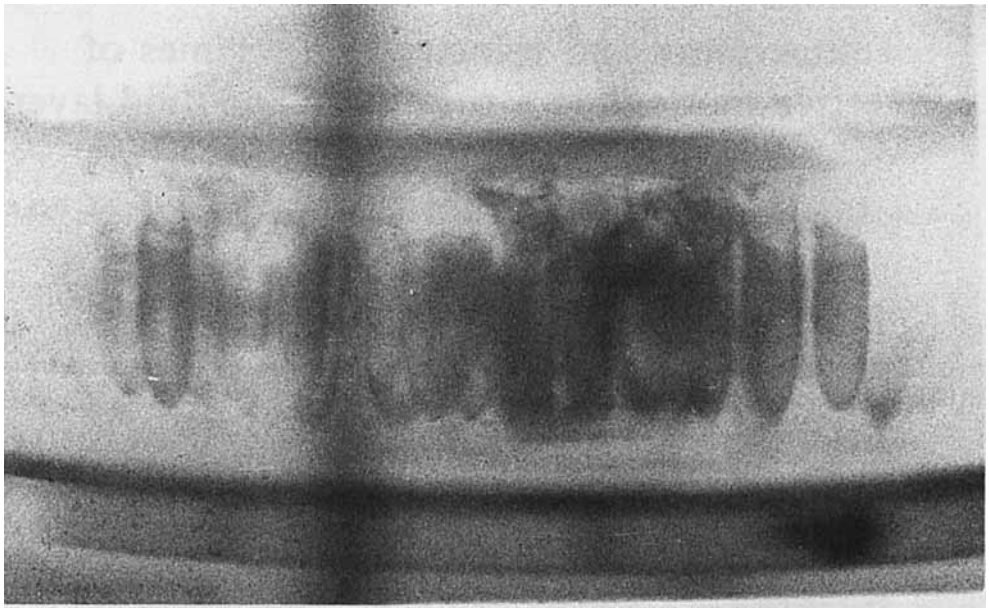

FIGURE 1. A photograph of the vortex cylinders along which the fluid is ascending in a rotating convecting fluid layer.

the fluid from the heated bottom layer, or leaving the upper surface of the fluid. The Rayleigh flux number Ra_f is related to the ordinary Rayleigh number by

$$Ra_f = RaNu, \quad Nu = \frac{fh}{\rho c_p k \Delta T}, \tag{1.2}$$

where the Nusselt number Nu characterizes the heat transfer through the layer with a temperature difference ΔT across it.

In Paper 1 we also considered non-stationary processes in the initial stage of convection, i.e. convective rings formed due to spin-up of the fluid which were transformed into regular vortex patterns of triangular symmetry. The individual elements of such a vortex lattice consist of a strong vortex sink in the middle surrounded by a cylindrical surface on which an ascending motion was observed. Owing to the poor contrast of our visualization technique it is difficult to see the latter motions on photographs presented in 1. In figure 1 we now present a picture where the cylinders with ascending motions can be seen. The irregular regimes are usually formed without the ring stage.

This paper, which is a continuation of a programme started in Paper 1, deals with motions that are steady in a statistical sense. It is organized in the following way. Section 2 classifies the various regimes of convection: state of rest, regular motions, and irregular motions which consist of geostrophical and non-geostrophical regimes. In §3 the temperature field measurements are described for the regular vortex grid and for irregular vortex regimes, the frequency spectra are presented both for cases of no rotation and rotation with different angular velocities, and an attempt is made to introduce a universal temperature spectrum for convection. Section 4 presents the measured velocity field for various convective regimes and §5 contains a summary and discussion of the main conclusions.

2. Classification of convective regimes in rotating fluids and transition boundaries between them

Chandrasekhar (1953) was the first to study the onset of convection in a rotating plane horizontal layer of fluid for a temperature difference prescribed at the boundaries and for slip or no-slip conditions on the velocity. Similar work was done by Nakagawa & Frenzen (1955) who also performed the first experimental test of the theoretically found relationships for the onset of the motions:

$$Ra_{\rm cr} = k_i Ta^{\frac{2}{3}} \tag{2.1}$$

for $Ta \geqslant 10^6$, where k_i is a numerical constant whose value is dependent on the type of boundary conditions. Recently Boubnov & Senatorsky (1988) studied a number of cases when the heat flux is prescribed at one or both boundaries with free or rigid upper or lower surfaces. In all cases relationships of the (2.1) type were found with the coefficient k_i being smallest, 2.39, for the case with the fixed heat flux at both boundaries are free upper and rigid lower surface, and largest for the prescribed temperatures with both surfaces free, 8.72, and both surfaces rigid, 8.09. We shall need these values later.

The second important transition is between the region of regular vortex motions studied in a detail in Paper 1 and the irregular vortex regime. It is a broad transition, with a factor of order two in values of Ra_f and Ta when moving across the transition curve, or more precisely, the region whose central line could be represented as

$$Ra_f(f_0/f) = k_1 Ta^{\frac{2}{3}} \tag{2.2}$$

where f_0 and k_1 are some constants – see figure 11 from Paper 1. There it was interpreted as a dependence of the ordinary Rayleigh number $Ra = Ra_f/Nu \propto Ra_f/f$ on the Taylor number $Ta^{\frac{2}{3}}$ – with the coefficient $k_1 \leqslant 33 \pm 8$. In the experiments which served as a base for deriving (2.2) the heat flux f was fixed at five values ranging from 85 to 1960 W m^{-2} and the fluid depth h and rotation rate Ω were changed. The fixing of the flux was performed by keeping the temperature of the water constant, from 20 °C to 60 °C where the value of the Prandtl number changed from about 7 to 3. At each value of f, and therefore Pr, the transition points were aligned parallel to $Ta^{\frac{2}{3}}$. This suggests another possible interpretation of these results (which came to our minds after the publication of Paper 1). The data (20 point) can be treated varying with Pr as $(Ra_f Ta^{-\frac{2}{3}})^{\alpha}$. For $\alpha = -0.2493$ this dependence was found to be linear with the correlation coefficient $r = 0.953$. Therefore the transition curve (b) (see figure 2 below) can be represented as

$$Ra_{fb} = C_1 Ta^{\frac{2}{3}} Pr^{-4} \tag{2.3}$$

with $C_1 = 2.62 \times 10^5$. Both interpretations seem to be possible at present because, as we see later (§3) isolines Nu = const on the plane $(\log Ra_f, \log Ta)$ are parallel $Ta^{\frac{2}{3}}$, at least for regular regimes.

One should be cautious in applying (2.3) to a wider range of, especially, Prandtl numbers. For instance, for the case of fixed heat flux at both boundaries and an upper free surface, when (2.1) holds with $k_i = 2.39$ the ratio of the right-hand sides of (2.1) to (2.3) is $2.39Pr^4/C_1$, being equal to 1 at $Pr = (2.62 \times 10^5/2.39)^{\frac{1}{4}} = 18.2$: i.e. at such a value of the Prandtl number both curves (2.1) and (2.3) coincide. Clearly relation (2.3) is not valid for $Pr \geqslant 10$ and the whole transition region in the space of parameters Ra_f, Ta and Pr should be determined more precisely. At the moment one

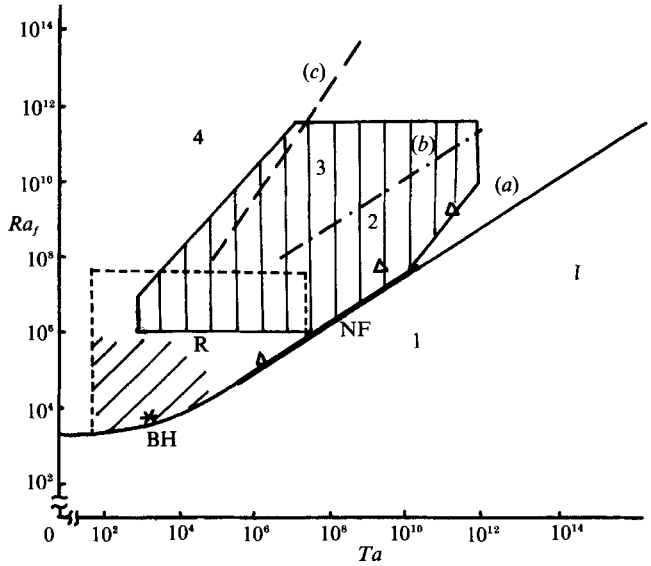

FIGURE 2. Diagram of different regimes in the plane (Ra_f, Ta): 1, thermoconductivity regime; 2, regular vortex grid; 3, irregular geostrophic turbulence; 4, thermal turbulence; (*a*) critical curve for convection onset; (*b*) curve of transition to the irregular regime for $Pr = 4.5$; (*c*) curve with $Ro = 1$ ($Pr = 4.5$). Thick solid line, NF, check of stability curve in experiments by Nakagawa & Frenzen (1955); BH, point from Busse & Heikes (1980), R, region studied by Rossby (1969). Region with vertical hatching is studied here and in Paper 1.

can only say that the transition from the regular vortex regime to an irregular one is through the region parallel to the first transition curve (2.1).

The region of irregular motions can be delineated by the requirement that the Rossby number

$$Ro \equiv V/2\Omega h = 1, \tag{2.4}$$

where V is a characteristic fluid velocity. For $Ro \ll 1$ we have geostrophic flow and for $Ro \geqslant 1$ the influence of the Coriolis force is small for the flow patterns.

Golitsyn (1980, 1981) used similarity arguments to show that in convective flows subject to the geostrophic constraint and for $4Nu \gg 1$ the scale of the velocity should be determined by the rate of the kinetic energy dissipation $\epsilon = \alpha g f/\rho c_p$ and the Coriolis parameter 2Ω. The arguments produced

$$V = C_2(\epsilon/2\Omega)^{\frac{1}{3}}. \tag{2.5}$$

This formula was verified in very crude measurements by Golitsyn (1981) and in more systematic measurements to be described here, in §4. Both works produce $C_2 \approx 2$. In terms of our external parameters the condition (2.4) taking (2.5) into account can be represented as

$$Ra_f \approx \tfrac{1}{4}Pr^2\,Ta^{\frac{3}{2}}, \tag{2.6}$$

where the coefficient $\frac{1}{4}$ is C_2^{-2}. So the inequality

$$Ra_f \ll 2^{-2}Pr^2\,Ta^{\frac{3}{2}} \tag{2.7}$$

is a condition of geostrophic convection.

Figure 2 presents the $(\log Ra_f, \log Ta)$-plane with these regions: 1 is the region of rest with (*a*) the critical curve for conditions of two rigid boundaries and a prescribed

temperature difference. The thick sector of curve (*a*) is that part of it checked by Nakagawa & Frenzen, labelled NF. The part of the plane enclosed by short-dashed lines, *R*, was studied by Rossby (1969) and the lower left part of it was also studied by him visually. The visual flow patterns were of rolls which depended only slightly on the Taylor number, but for the upper right part of this region Rossby noted that some rolls were superimposed by vortices of the type studied by Nakagawa & Frenzen (1955) and described in detail in Paper 1. The region studied here and in Paper 1 experimentally is shown by vertical hatching. The segment of a straight line (*b*) corresponds to (2.3) with $Pr = 4.5$ ($T = 38.5$ °C): it divides the regular regimes of region 2 from the irregular regimes above (2.2) – region 3. The segment of the line, (*c*), corresponds to (2.6) for the same value, $Pr = 4.5$. It separates the region of irregular geostrophic motions 3 from the region 4 where the motions are irregular but rotation is felt only weakly. The latter is the region containing the usual thermal turbulence. BH is the point where Busse & Heikes (1980) observed slightly unstable auto-oscillating rolls. These are major regimes of rotating convective layers for sufficiently large Taylor numbers. The boundaries between them need to be studied more precisely.

3. The temperature field

After the onset and development of convection in a vessel a regime develops corresponding to the boundary conditions. In our experiments these are prescribed heat flux at both boundaries and a free or rigid upper surface. The regular vortex grid, region 2 on the regime diagram of figure 2, can be described in some individual detail, such as the structure of each individual vortex, mean temperature profile etc. For the irregular regime, along with the mean profile, one can only consider various statistical characteristics of the temperature fluctuations.

All the experiments were carried out at the installation described in Paper 1 but with several additions and modifications. The cylindrical vessel from organic glass is filled with distilled water. The inner diameter of the vessel is 17 cm, the walls are 2 cm thick and the total height is 21 cm. The walls are additionally thermoinsulated by a foam plastic 7 cm thick. The bottom of the vessel is made of aluminium 3 cm thick and is heated by water from a thermostat. The whole system is placed on a turntable. The heat flux from the heated bottom comes through the fluid and leaves from its free surface due to evaporation, thermal radiation and contact with the colder laboratory air. This flux was determined in two ways: (i) by measured values of the water and air temperature and air humidity, as described in Paper 1, and (ii) by a thermocouple in the layer of epoxy at the bottom of the cylinder. Both determinations agreed within 5%. The cylinder axis coincides with the turntable axis and is parallel to g.

In a series of experiments to study the temperature field within the convective fluid an additional thermocouple is placed into fluid. In some cases both of its joints are fixed in space within the fluid and in other cases one joint is fixed and is in the thermostat outside the fluid and the second joint is either fixed within the fluid or can be moved within it. The thermocouples are made of nichrom and constantan wires of 50 μm in diameter, the length of the sensing part being 100 μm. Dynamical and thermal perturbations from such a thermocouple are negligibly small. To move one joint its wire is rolled up from one wheel to another through a system of blocks. The wheels are on axes which rotate with equal angular velocity from a common electromotor. The transitional velocity of the joint was always 1.71 cm/min =

$2.85\ 10^{-2}$ cm/s. The wheels were used only to measure the temperature profiles within the fluid, especially outside the lower thermal boundary layer. The lower wheel was placed at the bottom. To exclude its influence on the flow (though it is small) we put in this case into our vessel an intermediate Plexiglas bottom with a small hole for the wire. In this case the depth was measured from this new bottom.

The signal from the thermocouples comes to a preamplifier which is situated on the turntable because the direct transmission of a small signal through rotating current contacts leads to large distortions. The preamplified signal from the turntable goes to the recorder while the constant component of the current can be compensated, or recorded, depending on the aim of studies. The system can determine the temperature difference with an accuracy of 0.01 K. When the temperature-fluctuation power spectra are determined the fixed thermocouple is used and its amplified signal is fed into a computer. The frequency of the signal discretization is 32 Hz, the frequency pass band of the thermocouple is 0–10 Hz and the minimal resolved temperature difference in the coded signal is 0.01 K. The length of record analysed was usually 40 minutes.

3.1. *The temperature in a regular vortex grid*

3.1.1. *Temperature profiles*

Let us consider the main processes in the convection of a fluid with a free upper surface. A thermal boundary layer – cold film – is formed at the surface due to the IR sensible and latent heat fluxes. The film thickens with time, becomes unstable and then cold thermals are formed which descend. The problem has been studied in detail by Katsaros *et al.* (1977), Ginsburg, Golitsyn & Fedorov (1979) and many others. A conspicuous element of convective flow at large Rayleigh number, $Ra > 10^6$, is a strongly mixed core where the temperature hardly changes with height, the main temperature changes being within the boundary layers. Figure 3, curve 1, presents a typical temperature profile in turbulent convection for $\Omega = 0$. This profile can be divided into two parts: the upper one where there is the main temperature drop and the rest with $z_0 = 0.2 < z/h < 0.8$ where in the limits of measurement accuracy the temperature does not change (excluding the lower boundary layer).

If the fluid rotates with a constant angular rate Ω the irregular thermals for the case $\Omega = 0$ are replaced by intensive vortex sinks. In the regular vortex regimes the mean vertical temperature profiles are quite different. Some individual profiles are presented in figure 3, curves 2–5, for a layer 2.7 cm deep for the same flux, 150 W m^{-2}, showing the effect of increasing Ω from about $\frac{1}{6}$ to 1 revolution per second. The temperature in the upper (somewhat increasing) part of the fluid is also changing but less strongly than for the case $\Omega = 0$. In the main volume of the fluid the temperature gradient T_z is found to be proportional to Ω. A clearly linear vertical temperature profile is observed for smaller heat fluxes and larger rotation rates. This is caused by the fact that in this case perturbations created by the vortices are small owing to the rigid position of the vortices in the grid, and the temperature variations are small in the horizontal direction. We do not show the lower parts of curves 2, 4 and 5 in figure 3 because of the influence of the wheels. Curve 3 in figure 3 is a profile measured down to the bottom and shows that the lower thermal boundary layer is similar to the upper one. With the increase of the heat flux and fluid depth the main profile acquires considerable perturbations caused by horizontal inhomogeneity in the layer and each individual profile is distorted by these perturbations but on average they are still linear with height.

The dependence of T_z on the heat flux value was found to be very weak. Similarly,

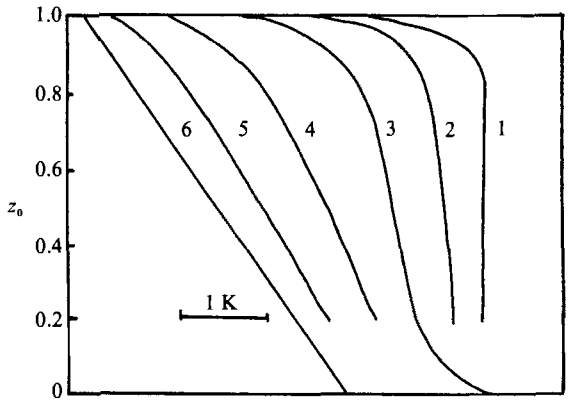

FIGURE 3. Vertical profiles of the mean temperature T for $h = 2.7$ cm, $f = 150$ W m^{-2}, $Ra_f = 2.7\ 10^6$: curve 1, $\Omega = 0$; 2, 1.04 s^{-1}; 3, 2.09 s^{-1}; 4, 4.18 s^{-1}; 5, 6.28 s^{-1}; 6, regime of conductivity.

the value of T_z seems to be independent of the non-dimensional height z/h, which means that $T_z \propto h^{-1}$. All these relationships for T_z may be satisfied by the following dimensional combination (note that the dimension of temperature can be introduced only through the buoyancy parameter αg):

$$T_z = C_3 \Pi, \quad \Pi = 2\Omega k Ra_f^{\frac{1}{2}} (\alpha g h^2)^{-1} = \frac{\Delta T}{h} Ra^{-1} Ta^{\frac{1}{2}} Ra_f^{\frac{1}{2}}, \tag{3.1}$$

where C_3 is a numerical coefficient. The main dependence will be on Ωh^{-1} because $Ra_f \sim h^4$ and the weak dependence on the heat flux in our experiments was nearly compensated by the dependencies of the molecular coefficients on the mean temperature of the water. All measurements were carried out for each of the three heat fluxes 150, 450 and 1650 W m^{-2}, depths 2.7, 5 and 10 cm, and angular velocity rates of 1.04, 2.09, 4.18 and 6.28 s^{-1}. Using these data we found that $C_3 = 2.21$ with the coefficient of the correlation between measured T_z and calculated Π being $r = 0.989$ for 21 pairs of points. The high value of r suggests that our guess for the structure of Π is about right (coefficient C_3 may be a weak function of Pr).

3.1.2. *The heat transfer through the layer*

The Nusselt number $Nu = fh/\rho c_p k \Delta T$, where ΔT is the temperature difference across the layer, can also be interpreted as the ratio of the 'eddy' heat transfer coefficient K_T to the molecular one, k:

$$Nu = \frac{K_T}{k}, \quad K_T = \frac{fh}{\rho c_p} \Delta T \leqslant \frac{f}{\rho c_p} T_z. \tag{3.2}$$

The inequality here is due to the fact that $\Delta T/h \geqslant T_z$ because here we disregard the thermal boundary layers.

Substituting (3.1) into (3.2), after some manipulations we find that $Nu = C_3^{-1} Ra_f^{\frac{3}{4}} Ta^{-\frac{1}{2}}$. Since $Ra_f = Ra\,Nu$ we find finally that

$$Nu = C_4 Ra^3 Ta^{-2}, \quad C_4 \leqslant C_3^{-4} = 4.17 \times 10^{-2}. \tag{3.3}$$

This rather complicated law for the heat transfer can be checked, at least partially, by the experiments of Rossby (1969). From (3.3) it follows that isolines $Nu = \text{const}$

on a graph with axes ($\log Ra, \log Ta$) should be straight lines with slope $\frac{2}{3}$ ($Ra \propto Ta^{\frac{2}{3}}$); hence, they are parallel to the isoline $Nu = 1$ which is the critical curve for convection onset. Rossby (1969) experimentally measured the values of $Nu = Nu(Ra, Ta)$ and found that with logarithmical axes (Ra, Ta) the isolines $Nu = \text{const}$ tend to be parallel to the theoretical stability curve $Ra_{cr} \propto Ta^{\frac{2}{3}}$. So our empirical heat transfer equation (3.3) agrees, at least qualitively, with direct experiments by Rossby (1969) and with the theoretical stability curves.

From (3.3) it follows that at $Nu = 1$, i.e. at the moment of convection onset, $Ra_f = Ra = C_3^{\frac{4}{3}} Ta^{\frac{2}{3}} \approx 2.88\, Ta^{\frac{2}{3}}$. But according to our numerical results for the boundary conditions of our laboratory experiments it should be $Ra_{cr} = 2.39 Ta^{\frac{2}{3}}$. Hence, the difference between the empirical constant 2.88 and the theoretical one, 2.39, has an accuracy of better than 20%. The sign of the difference also agrees with the inequality (3.3). From (3.3) it also follows that Nu isolines should be separated by a distance proportional to $Nu^{\frac{1}{3}}$. Treatment of data kindly sent to us by Professor H. T. Rossby shows that the isolines are nearing each other and for his maximal value $Ta_{max} = 3 \times 10^7$ the exponent δ_1 in the relationship $l \propto Nu^{\delta_1}$, where l is the distance between the isolines, is $\delta_1 = 0.45$. However, a tendency to a further closing together of the lines is obvious from his data and his figure 10. We should point out that our experiments to obtain (3.3) were in the range $3 \times 10^6 < Ra_f < 4 \times 10^9$ and $7 \times 10^6 < Ta < 5 \times 10^{10}$, i.e. regular or slightly irregular regimes.

Naturally the value of T_z is limited because it cannot exceed the value due to purely molecular conductivity in the case of no motion when the internal gradient equals the external one, $\Delta T/h$. This limitation is shown in figure 3 by curve 6. All the profiles in figure 3 were measured at the axis of our cylinder; however, some experiments were carried out at distances 1.2 and 3.5 cm from the centre and showed that the profiles $T(z)$ did not depend on that distance.

It should be noted that the relationship $Nu \propto Ra^3 Ta^{-2}$ was first obtained theoretically by Chan (1974) for two free boundaries and in the approximation $Pr \to \infty$ for the range of Taylor numbers $O(Ra^{\frac{4}{3}}) \leqslant Ta \leqslant O(Ra^{\frac{3}{2}})$ which is equivalent to $Ta^{\frac{3}{4}} \geqslant Ra \geqslant Ta^{\frac{2}{3}}$. The relationship was specified by Riahi (1977) who, for these boundary conditions, calculated the numerical coefficient to be equal to 0.0052. At $Nu = 1$, i.e. on the critical curve, we have then $Ra_{cr}/Ta^{\frac{2}{3}} = 0.0052^{-\frac{1}{3}} = 4.52$ instead of 8.72 according to exact calculations by Chandrasekhar (1953, 1961). It thus apparently follows that to extrapolate (3.3) into a weakly supercritical region is not readily possible and the heat transfer through that region just above the critical curve needs to be elucidated. Perhaps the limit $Pr \to \infty$ also plays a role in this disagreement between the numerical coefficients.

One can develop arguments which suggest that the relationship $Nu \propto Ra^3 Ta^{-2}$, or a similar one, may be appropriate for the whole region 3 (figure 2) of geostrophic convection. For very large values of Ra_f, or Ra, and Ta it is natural to expect $Nu \propto Ra^m Ta^{-n}$ with $m, n > 0$. If we assume that the heat flux f does not depend on h and the isolines $Nu = \text{const}$ are slightly steeper than curve (a) of figure 2, i.e. proportional to $Ta^{\frac{2}{3}+\delta}$, $\delta > 0$ (if $\delta < 0$ the isolines would cluster near a), then to determine m and n we have a system

$$3m - 4n = 1, \quad n = m(\tfrac{2}{3} + \delta).$$

The solution is $m = 3(1-12\delta)^{-1}$, $n = (2+3\delta)(1-12\delta)^{-1}$. To have both $m, n > 0$ we must have $\delta < \frac{1}{12}$, i.e. Nu isolines should be less steep than $Ta^{\frac{3}{4}}$. Note that here the temperature difference

$$\Delta T \propto (f\Omega^{2n})^{1/(m+1)}$$

depends much more weakly on the heat flux than in the case $\Omega = 0$ when $\Delta T \propto f^{\frac{3}{4}}$ if $Nu \propto Ra^{\frac{1}{3}}$.

We wish to stress that (3.3) implies that the heat transfer is proportional to the fourth power of the temperature difference. Unfortunately, we were not able to make direct measurements of the heat transfer in our experiments but our treatment of the Rossby data implies that in his experiments he has obtained the relationship $f \propto \Delta T^{n+1/\delta_1} = \Delta T^{3.22}$. All this opens interesting possibilities in regulating the heat transfer through rotating fluid layers, because from (3.3) it follows that $f \propto \Delta T^4 \Omega^{-4}$. Clearly, the heat transfer through a convecting and rotating fluid layer should be studied directly and for a much wider range of Ra and Ta than here, together with the structure of the thermal boundary layers, but our present equipment is not suited for this task.

3.2. *Horizontal temperature profiles*

Horizontal temperature distributions were measured in two ways which give the same results. Either the thermocouple was moved within the fluid as in the studies of the vertical structure or one joint of the thermocouple was fixed at some distance, R, from the centre where the second joint was. The last method uses the fact that the water in the cylinder rotates very slowly, retarding relative to the walls owing to the friction of the water surface on the air (this influence of the air was observed even for a height of the cylinder walls up to 50 cm above the surface; the rate of this rotation is usually more than two orders of magnitude slower than the basic rotation Ω). To remove this air–water interaction a wire net was used as a shield above the cylinder, which did not interfere with evaporation but removed the air velocity shear at the water surface. With such a shield the vortex grid is at rest relative to the walls, otherwise there is a slow motion of the whole vortex grid relative to the cylinder walls.

Figure 4 presents parts of the temperature records at a point with $R = 1.5$ cm from the central axis at different levels from $z_0 = 0.02$. The water depth here is $h = 5$ cm, and $f = 450$ W m^{-2}, $\Omega = 6.28$ s^{-1}. The fluid depth is measured at $\Omega = 0$ and when calculating the non-dimensional vertical coordinate z_0 the value of h used took into account the parabolic meniscus forming at rotation. In this case $Ra_f = 1.67 \times 10^8$, $Ta = 2.33 \times 10^9$, the distance between the almost regular vortices being $d = 1.03$ cm. The whole grid rotates with period 6 min 35 s and owing to the absence of the shield spatial temperature fluctuations are apparent. Near the upper evaporating surface, $z_0 = 0.98$, the sinking of the colder water prevails in a narrow region around the vortex centre. The upward motion of the warmer fluid forms a background. The distance between the minima of the record corresponds to the spatial distance between two vortices which may be crossed at a periphery, so values of minima should differ. Near the lower boundary $z_0 = 0.02$ the ascent of warmer fluid prevails, but maxima of the temperature record correspond here not to the vortex centre, but to the passage of the cylindrical surface surrounding vortices (see figure 1) where the warmer fluid ascends; hence two temperature maxima correspond to one vortex.

Records similar to those in figure 4 were treated statistically for various depths. Figure 5 presents the dependence on z_0 of the r.m.s. temperature fluctuations σ_T and the third moment $\gamma_T = \overline{(T-\bar{T})^3}\,\sigma_T^{-3}$, non-dimensionalized by σ_T. The largest values of σ_T are observed in the boundary layers near the surface and the bottom, for $0.4 < z_0 < 0.9$ there is a small decrease of σ_T with depth and for $0.1 < z_0 < 0.3$ it starts to increase slightly. Disregarding these small changes we can say that the main volume, for $0.1 < z_0 < 0.9$, has almost constant temperature fluctuations.

The change of sign of the third moment, non-dimensionalized by σ_T, reflects the

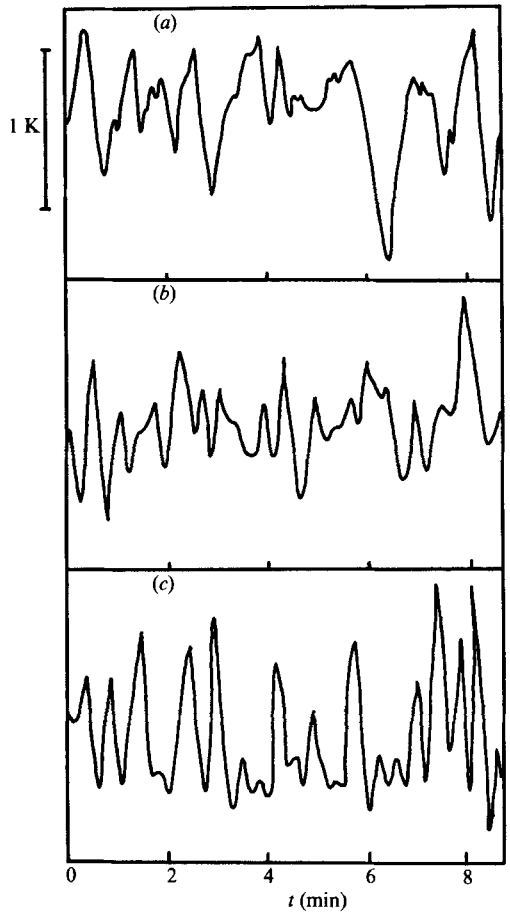

FIGURE 4. Parts of records of the horizontal time section of temperature taken 1.5 cm from the vessel centre for the regular regime ($f = 450$ W m^{-2}, $\Omega = 6.28$ s^{-1}, $h = 5$ cm, $Ra_f = 1.6 \times 10^8$, $Ta = 2.3 \times 10^9$). The different horizontal positions are: (*a*) $z_0 = z/h = 0.98$, (*b*) $z_0 = 0.51$, (*c*) $z_0 = 0.02$.

difference in horizontal temperature structure at various levels discussed in relation to figure 4.

The mean temperature difference ΔT_h between the vortex core and its surroundings depends only weakly on the rotation rate and the total fluid depth. The main dependence observed is upon the heat flux f. In one experiment at a distance 1 cm from the bottom for the fluxes 150, 450 and 1650 W m^{-2} the values of ΔT_h are 0.53, 0.88 and 1.47 K which may be approximated by the dependence $\propto f^{0.4}$.

Summing up, our experiments reveal the following distribution of temperature in the regime of the convective vortex grid. The mean temperature linearly decreases with depth with the gradient determined by (3.1). Horizontally the temperature varies more or less periodically in space from the cold vortex core to the warmer enveloping cylinder.

3.3. *The spectrum of irregular convection in a non-rotating case*

We put this material here because it serves as a reference point for the temperature frequency spectra of convection with rotation and also because studies of the usual turbulent laboratory convection at $\Omega = 0$ are not numerous and we have found some

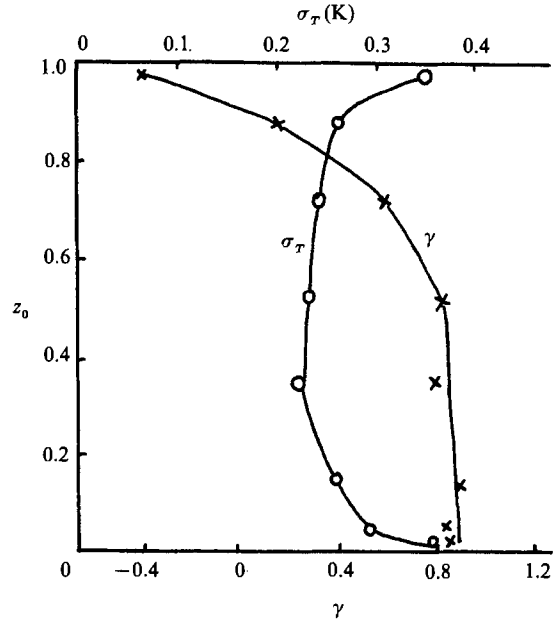

FIGURE 5. The dependence of the temperature variance σ_T, and skewness γ_T on $z_0 = z/h$ for a regular convective grid.

universal relationships not described before. As already mentioned, and is well known, for irregular convection the mean temperature within the fluid is constant with height and changes only in the boundary layers. The main characteristics of the temperature field in the bulk of the fluid are the statistical properties of the temperature fluctuations relative to this mean temperature value. Here we shall mainly be concerned with the temperature spectrum and its variance.

One popular model to describe turbulent convection is that by Howard (1963) and its modifications. The model states that motion within the fluid is forced by the processes in the boundary layers. At the fluid boundary the molecular thermoconductivity causes the formation of a boundary layer which grows with time under conditions of heat supply (or loss), becomes unstable and breaks up releasing thermals, then it is restored and the process repeats. The process is rather irregular but it can be characterized by the most probable value of the time period, τ. The value of τ is determined by the following relationship (Foster 1969; Ginsburg *et al.* 1979; Golitsyn 1979):

$$\tau = C_5(\nu\rho c_p/\alpha g f)^{\frac{1}{2}} = C_5 h^2 k^{-1} Ra_f^{-\frac{1}{2}}. \tag{3.4}$$

Foster & Waller (1985) have studied the temperature power frequency spectra measured 1 cm from the heated bottom within a water layer 25 cm deep. The maxima of these spectra correspond to a period which agrees well with (3.4) and $C_5 = 12.4$. The value of the same coefficient determined by a different method by Ginsburg *et al.* (1979, see also Golitsyn 1979) was found to be 12.7 ± 1.4.

We checked (3.4) by changing the depth from 2.7 to 20 cm. The spectra for temperature fluctuations $S_T(\omega)$ are presented in figure 6, where the ordinate measures ωS_T as a function of the logarithm of frequency ω. In such a representation the area under the curve $\omega S_T(\omega)$ for a given frequency interval (ω_1, ω_2) represents the contribution of this interval to the total variance. The spectra here are for $f =$

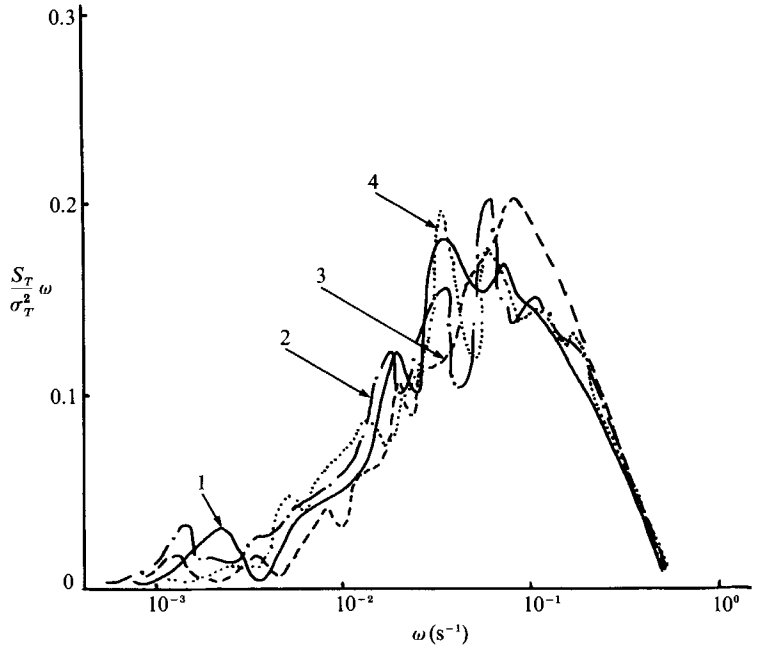

FIGURE 6. Spectra of the temperature fluctuations $\omega S_T(\omega)$ for $\Omega = 0$, $f = 1650$ W m^{-2}: curve 1, $h = 2.7$ cm; 2, 5 cm; 3, 10 cm; 4, 20 cm.

1650 W m^{-2} and different depths. Despite the last fact the spectra, within the limits of statistical uncertainty, are close to each other. The largest differences are for low frequencies where the main contribution is from large-scale flows whose scales are comparable with the vessel size. Note that ω here is the usual, not angular, frequency and the length of record used to calculate spectra was about 40 minutes.

The characteristic viscous time is $t = h^2\nu^{-1}$. The non-dimensional period τ_0 corresponding to the most probable frequency ω_0 can be written as $\tau_0 = \omega_0^{-1}h^{-2}\nu$. The value of ω_0 is determined by finding the centre of the segment of the line which intersects the curve $\omega S_T(\omega)$ at half of the maximum level (in normal, not logarithmic coordinates). Figure 7 shows the dependence of τ_0 on Ra_f for three values of the heat flux: 150, 450 and 1650 W m^{-2}, and four depths: $h = 2.7$, 5, 10 and 20 cm. The stars are data from Foster & Waller and other points are ours. The straight line corresponds to (3.4) with $C_5 = 12.7$.

Foster & Waller (1985) gave in their figure 3 the temperature spectra for f from 30.8 to 1970 W m^{-2} as $S_T(\omega)$. For four values of f, each exceeding the preceding one fourfold, these spectra are of similar shape and are equally spaced along the abscissa $\log\omega$. The authors were concentrating on checking equation (3.4), but their results hint that there could be coordinates for which all the spectra would be identical. We have chosen as the ordinate $S_T/\sigma_T^2\tau$ and as the abscissa $\omega\tau$. With such coordinates all the four spectra coincided when we took their smoothed values.

In our experiments the spectra were obtained for four depths and three heat fluxes as described for the most probable period in figure 7. As in the case of Foster & Waller (1985) our thermocouple was also 1 cm above the bottom at most cases. These spectra in the coordinates described are presented in figure 8. The dashed line is the common curve for the spectra by Foster & Waller (1985) and the results by Kirdyashkin & Semenov (1983). For $h = 2.7$ cm the spectrum is shifted toward lower

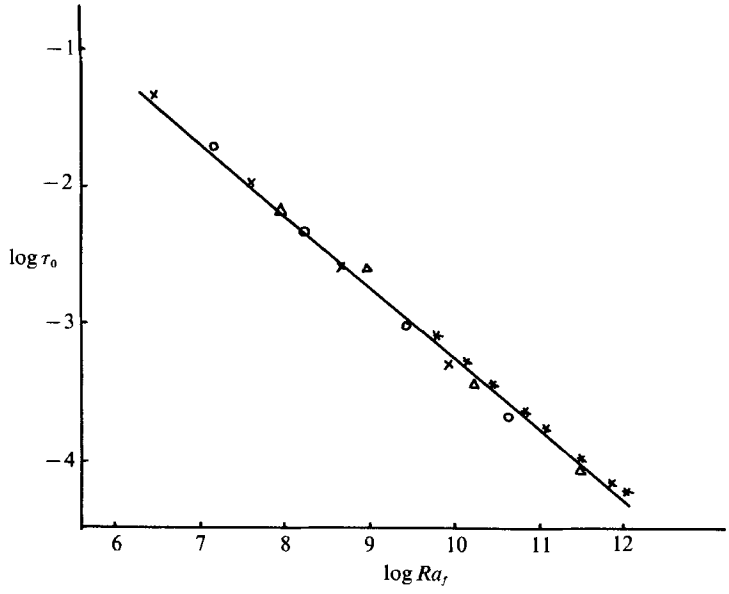

FIGURE 7. Dependence of the most probable period of temperature fluctuations τ_0 on Ra_f: ×, $f = 150$ W m^{-2}; ○, 450 W m^{-2}; △, 1650 W m^{-2}; *, results from Foster & Waller (1985).

frequencies and in figure 8 it is given by the thin solid curve for the lowest heat flux 150 W m^{-2} when $Ra_f = 2.7 \times 10^6$. It clearly shows that the turbulent convection for such a Rayleigh number is not sufficiently developed. The universal spectral dependence is observed starting with $Ra_f > 3 \times 10^7$.

The spectra were also measured at various points within the fluid. It was found that their shape and the amplitude did not significantly depend on the position where the temperature is measured, in agreement with the approximate independence of the temperature variance with height (see figure 6). The spectra of convective temperature fluctuations have been measured by a number of authors (see Deardorff & Willis 1967; Fitzjarrald 1976; Zimin & Ketov 1978; Gurvich & Yurchenko 1980; Kirdyashkin & Semenov 1983). Their spectra at sufficiently large Rayleigh numbers are similar to ours, but interpretations differ. For instance, most of the spectra in the first two papers are for insufficiently large Rayleigh number and are the spatial spectra measured by moving the sensor along their chamber, but with increasing Ra they approach ours. Zimin & Ketov proposed two spectral intervals where $S_T(\omega)$ was proportional $\omega^{-\frac{5}{3}}$ and ω^{-4} but the intervals were too short and subjectively chosen, and their spectrum was identical to ours in figure 8. Gurvich & Yurchenko (1980) proposed $S_\tau \sim \omega^{-2}$ using some dimensional arguments but a closer inspection of their graph shows deviations at the end of the line with slope −2. Kirdyashkin & Semenov (1983) proposed a universal spectrum for convection near a heated vertical wall but the frequency normalizing factor chosen was not the external one, as here, but a purely internal one obtained in the data treatment process. But their spectrum is also identical to ours. All this speaks in favour of a hypothesis that the power frequency spectrum of convective turbulent fluctuations has a universal form over a broad range of Rayleigh numbers, independent of the means of convection generation. These spectra do not obviously have any power ranges, however we cannot exclude that such intervals could appear at much larger sizes of vessels, i.e. at much larger values of the Rayleigh number.

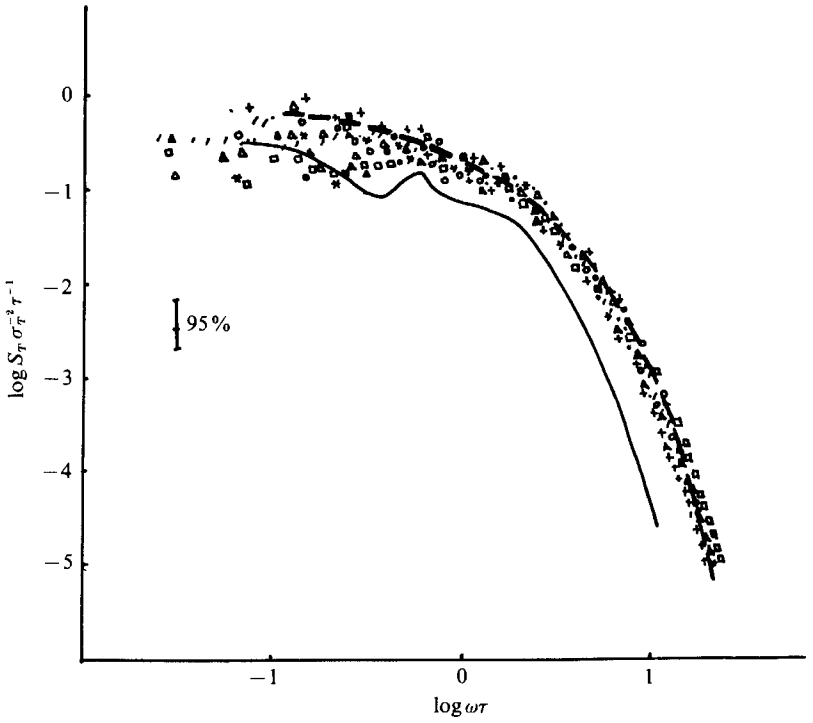

FIGURE 8. The universal convective temperature time spectrum for $\Omega = 0$ in coordinates $S_T \tau^{-1} \sigma_T^{-2}$, $\omega\tau$. For $h = 5.0$ cm: ●, $f = 150$ W m^{-2}; △, 450 W m^{-2}; +, 1650 W m^{-2}; for $h = 10$ cm: ○, $f =$ 150 W m^{-2}; □, 450 W m^{-2}; ı, 1650 W m^{-2}; for $h = 20$ cm: *, $f = 150$ W m^{-2}; ▲, 450 W m^{-2}; ■, 1650 W m^{-2}; ——, $h = 2.7$ cm, $f = 150$ W m^{-2}; – – –, results by Foster & Waller (1985); Kirdyashkin & Semenov (1983) spectrum is indistinguished at this scale from the latter one.

Irregular convection in a plane fluid layer is characterized by the fact that all its statistical parameters can be expressed in terms of external parameters not only in case $\Omega = 0$ (Deardorff 1970; Fitzjarrald 1976) but also for the geostrophic case (see §3.4 below). The temperature variance in these cases, outside the boundary layers, is almost independent of the vertical coordinate z, differing from the case of free convection above a plane where (Prandtl 1932; Oboukhov 1960)

$$\sigma_T = C_6'(f/\rho c_p)^{\frac{2}{3}} (\alpha g z)^{-\frac{1}{3}}.$$

For a plane layer it is natural to take instead of z its height h, multiplying σ_T by $f_1(z/h)$. The function f_1 differs from unity only at the boundary layers. According to Deardorff & Willis (1967, figures 6–8) and to our figure 9 the function f_1 increases by some 30–70% within the boundary layers depending on the value of Ra. Therefore the variance can be scaled as

$$\sigma_T = C_6(f/\rho c_p)^{\frac{2}{3}} (\alpha g h)^{-\frac{1}{3}}. \tag{3.5}$$

This formula can be transformed into a non-dimensional form (Fitzjarrald 1976):

$$\sigma_T/\Delta T = C_6 Nu\,(Nu\,Ra\,Pr)^{-\frac{1}{3}}. \tag{3.6}$$

According to him, for air $C_6 = 0.98 \pm 0.05$, but Deardorff (1970) gives $C_6 = 1.9 \pm 0.1$. Our nine points ($h = 5$, 10 and 20 cm, $f = 150$, 450 and 1650 W m^{-2}) measured 1 cm from the bottom (at two points separated by 3 cm) produce $C_6 = 2.4$

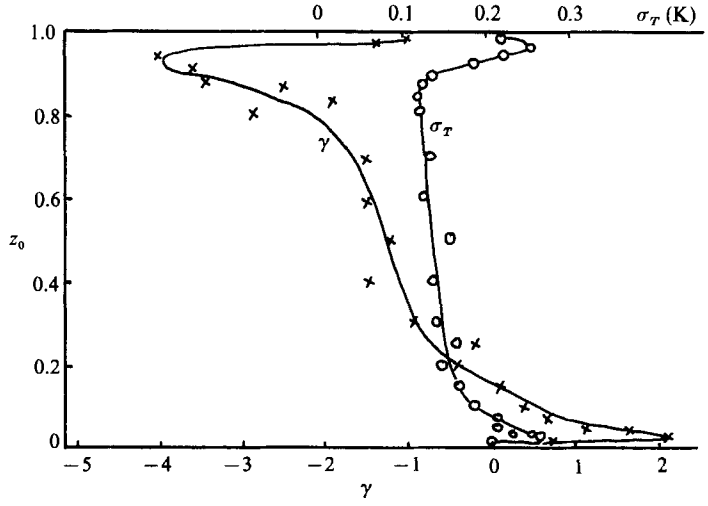

FIGURE 9. Dependence on $z_0 = z/h$ of the temperature variance σ_T and skewness γ_T, for $Ra_f = 4.1 \times 10^{10}$, $\Omega = 0$.

with a correlation coefficient $r = 0.980$. The general structure of (3.5) seems to be well confirmed. The difference in the values of the numerical coefficient can be related to the different heights of measurements: we took ours near the upper surface of the lower boundary layer, whereas Deardorff & Willis (1967) measured in the middle of the air layer as did Fitzjarrald (1976). The last author discussed the difference between his results and those by Deardorff & Willis but could not explain it. If we reduce our value of C_6 by a factor 1.5 ± 0.2 (which is the ratio between value of σ_T measured at one point and σ_T for the difference of the signals measured at two points within the fluid) we obtain $C_6 = 1.6 \pm 0.5$. Clearly further work is needed to determine this coefficient more precisely.

Figure 9 presents the dependence on z_0 of the second and the third moments of the temperature fluctuations for $h = 20$ cm and $f = 450$ W m^{-2}. The non-dimensional third moment γ_T characterizes here a ratio between the intensities of the rising warmer water and the sinking colder water. Near the bottom the rising warmer thermals are formed and $\gamma_T > 0$. Near the surface $\gamma_T < 0$ and in absolute value it is much larger than that below, which reflects the fact that the colder thermals formed from the cold film at the upper surface are more intense than the warmer thermals formed at the lower heated boundary. Note some similarities between figures 5 and 9, i.e. the behaviour with height of the temperature variance does not significantly depend on whether the system is at rest or rotating.

3.4. *The influence of rotation on the statistical characteristics of turbulent convection*

The temperature fluctuations, as in §3.2, were measured by two thermocouples. The first thermocouple (used for measuring all the spectra) had one joint within the fluid 0.9 cm above the bottom on the axis of the cylinder and the other joint in the thermostated water outside the vessel. The first joint of the second thermocouple was placed at the cylinder axis 1 cm above the bottom and its second joint was at the same height but 3 cm off the axis. The second thermocouple (used for qualitative analysis of the spatial temperature structure) owing to the fluid rotation when there is air shear allowed measurement of a horizontal circular section of the fluid with diameter of 6 cm. The thermocouples could also be moved vertically, and the mean

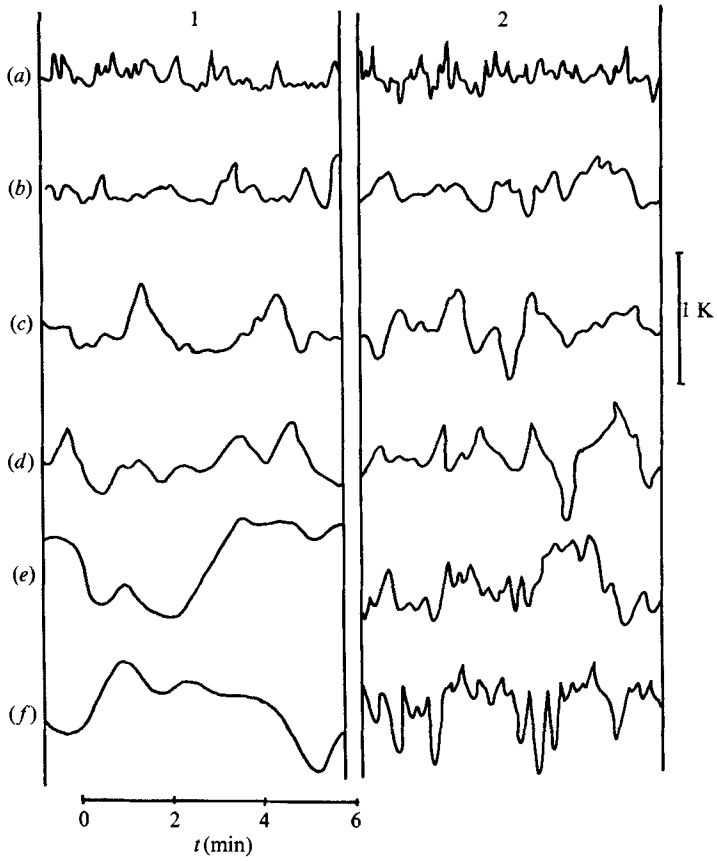

FIGURE 10. Records of the temperature fluctuations for different Ω, at $f = 150$ W m^{-2}, $h = 10$ cm, $Ra_f = 5.1 \times 10^8$: (*a*) $\Omega = 0$; (*b*) 0.52 s^{-1}; (*c*) 1.05 s^{-1}; (*d*) 2.09 s^{-1}; (*e*) 4.19 s^{-1}; (*f*) 6.28 s^{-1}.

vertical temperature profiles for turbulent convection with rotation were similar to those at rest (see curve 1 of figure 3), i.e. constant temperature within the bulk of the fluid with sharp changes in the boundary layers.

Figure 10 shows temperature records from the two thermocouples for different rotation rates Ω. On an increase of the Taylor number Ta a transition is evident to more regular low-frequency temperature changes. However, there is no approach to a stationary pattern, which possibly is related to the vortex grid oscillations relative to its state of rest. In regular grids the distance between the vortices is of order 0.5 cm and the grid oscillations, even with a small amplitude, could be recorded as noticeable temperature changes at a fixed point. A decrease in the characteristic period in the record of the thermocouple 2 (right part of figure 10) corresponds to the increase of the rotation rate Ω and subsequent decrease of the distance between the vortices (as $\Omega^{-\frac{1}{2}}$ in irregular regimes and $\Omega^{-\frac{1}{3}}$ in the regular ones, see Paper 1).

The records, 40 minutes long for cases when there were no swirls of the fluid, were treated and their power spectra were obtained. As Ta increases, the spectra narrow and shift to lower frequencies and their maxima increase. The position of the spectral maximum depends on the position of the regime in question on the (Ra_f, Ta)-diagram relative to the critical curve of convection onset.

When considering normalized spectra $\sigma_T^{-2} S_T(\omega)$ one should recall the regime

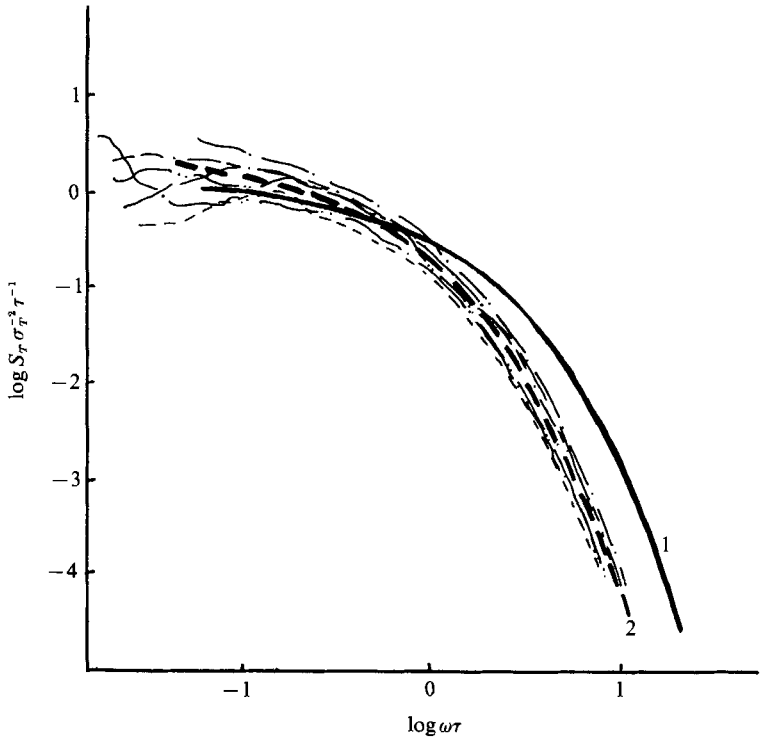

FIGURE 11. Spectra $S_T \sigma_T^{-2} \tau^{-1}$ for different Ω. Curve 1, $\Omega = 0$ (figure 8); curve 2, mean spectrum for geostrophic turbulence averaged over 26 individual spectra, all of which are within the dashed limits shown.

diagram of figure 2 and the geostrophical condition (2.6). If we are at the transitional region $Ro \sim 1$ on the plane (Ra_f, Ta), then as the rotation increases there is a gradual shift of the spectrum toward the left without changing its shape. If $Ro < 0.1$ then again with no change of shape the spectrum shifts toward the new 'stationary' form curve 2 of figure 11. Twenty-six spectra are presented in an averaged form from region 3 of figure 2 satisfying condition $Ro < 1$. Spectrum 2 of figure 11 can be transferred into spectrum 1 of the same figure or into the universal spectrum of convection at $\Omega = 0$ if we replace τ by $\tau_1 = C_7 \tau$ where $C_7 = 3.0 \pm 0.4$. For the case $\Omega = 0$ the value of $\tau \approx 12.4 h^2 \nu^{-1} Ra_f^{-\frac{1}{2}}$ was a basic period of instability of the thermal boundary layers. Our last result shows that in the region of geostrophic irregular convection this basic timescale remains qualitatively the same, only the numerical constant is about half an order of magnitude larger. It is also interesting to note that the shape of the geostrophic irregular convection universal spectrum $\sigma_T^{-2} S_T(\omega\tau_1)$ does not explicitly depend on the rotation rate Ω, apart from the value of the temperature variance σ_T^2.

The value of σ_T^2 can be estimated theoretically from several lines of arguments. First, from dimensional arguments: disregarding molecular coefficients and the fluid depth for irregular motions we are left with the kinematic heat flux $f' = f/\rho c_p$, Ω and the buoyancy parameter αg. From these we have

$$\sigma_T^2 = C_8 \Omega f'/\alpha g. \tag{3.7}$$

The same result can be obtained from the thermal wind equation in the convecting layer taking into account the velocity scale (2.5). The third line comes from the

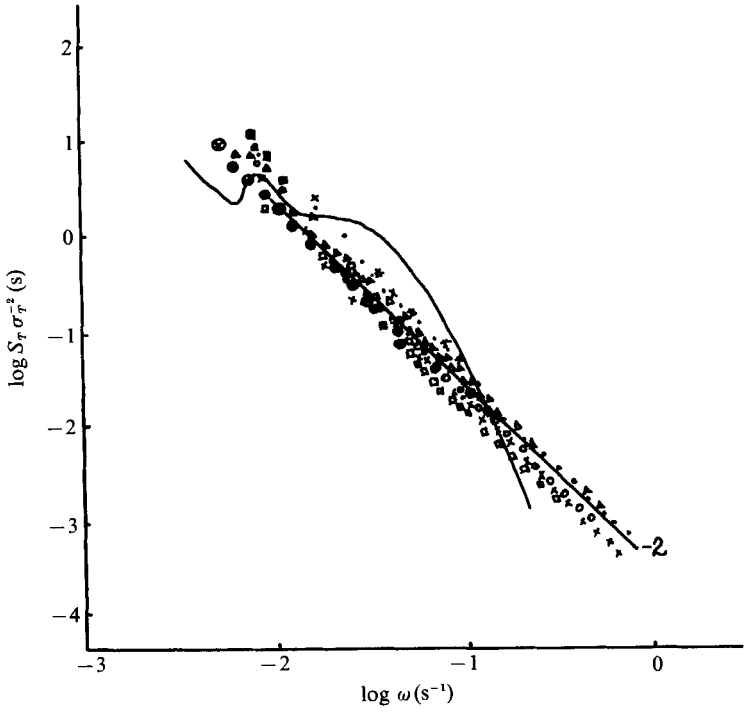

FIGURE 12. Spectra $S_T \sigma_T^{-2}$ in seconds for small flux $f = 150$ W m^{-2}. For $h = 2.7$ cm: ——, $\Omega = 0$; □, $\Omega = 0.209$ s^{-1}; ●, 0.52 s^{-1}; *, 1.05 s^{-1}; △, 2.09 s^{-1}; ○, 4.18 s^{-1}; ×, 6.28 s^{-1}. For $h = 5$ cm: ▲, $\Omega = 2.09$ s^{-1}; ⊗, 6.28 s^{-1}. For $h = 10$ cm; ■, $\Omega = 6.28$ s^{-1}.

expression $f' \propto \sigma_T \sigma_u$, where σ_u is the r.m.s. of velocity fluctuations whose dependence on the external parameters is given by (2.5). The formula (3.7) was checked by the 26 available values of σ_T^2 measured in region 3, irregular geostrophic convection. The correlation coefficient between the experimental value of σ_T^2 and $\Omega f'/\alpha g$ was $r = 0.984$ and the regression coefficient $C_8 = 0.42$.

In the region of almost regular quasi-steady structures the spectrum $S_T(\omega)\,\sigma_T^{-2}$ has a different form, as presented in figure 12. It has a very well-pronounced range over two decades where $S_T(\omega) \propto \omega^{-2}$. This behaviour could be explained by simple dimensional arguments supposing that the temperature power frequency spectrum $S_T(\omega)$ with dimension $\Theta^2 T$ is determined only by the rate of temperature inhomogeneity dissipation N (dimension $\Theta^2 T^{-1}$), as for the temperature turbulent spectrum (Oboukhov 1949; Corrsin 1951), and by the frequency ω. Then we at once obtain $S_T(\omega) = \alpha_1 N \omega^{-2}$ where α_1 is a constant. We must confess that any degree of rigour in this kind of argument would require a very substantial study which should answer, along with many others, such questions as why such a spectrum is observed only for almost regular vortex regimes, why there is no trace of rotation in that simple form, etc. However, we have mentioned it here only because it seems to be of considerable significance.

4. The velocity field

For studying the velocity field two mutually complementary methods were used. The first was used to study vertical velocities in the regime of a regular convective

grid and consists in measuring the velocity of dye propagation. In this regime the colder fluid from the upper surface layer descends within a narrow vortex which serves as the axis for a cylinder on which the warmer fluid ascends. The latter motion is seen in figure 1. The dye is bromthymole blue and it is placed at the fluid surface (other examples of motion patterns visualized in this way can be found in Paper 1). Maximal vertical velocities are observed in the vortices wherein the fluid comes only from the cold surface film. To measure these vertical velocities, horizontal lines 1 cm apart were drawn on the sidewalls and the time for dye to pass between the lines was measured. For a fluid 20 cm deep up to 18 such measurements can be made (boundary layers should be excluded). The dye is introduced to the surface about 20 minutes after the start of rotation in order to show a stationary pattern. For each set of external parameters five measurements were performed and their mean was taken.

The second method is also traditional. It uses small (about 20 μm) particles of aluminium powder filling the fluid which is illuminated by a narrow plane beam of light 2 mm wide. The tracks of particles are photographed with time exposure from 0.5 to 10 s. The same regime was photographed with several exposures to exclude particles leaving the beam during the exposure. Only those tracks were used whose length was directly proportional to the exposure time. The velocity is determined from the track length and exposure. This method gives good results for irregular regimes but identifies intense narrow flows badly.

4.1. *The regular vortex grid*

The velocity measurements were carried out for depths $h = 5$, 10 and 20 cm, heat fluxes $f = 150$, 450 and 1650 W m^{-2} and rotation rates $\Omega = 3.14$, 4.19, 5.24 and 6.28 s^{-1} (periods 2, 1.5, 1.2 and 1 s) and those cases where the regular grid was observed are considered here. The lower limit in depth is caused by difficulties in clear dye front determination at small depths, and the lower limit in Ω by the absence of a regular vortex grid for $\Omega < 3.14$ s^{-1}. The motion outside the boundary layers is considered because there the dye propagation is irregular (the front starts to form at the top and breaks up near the bottom).

Inside the vortex one can determine the vertical velocity w. The main characteristics of the value of w are as follows: it does not depend on the vertical coordinate z, i.e. it is constant within the fluid, and only very weakly depends on Ω, decreasing with Ω; it decreases with the approach to the critical curve of a regime, the main determining factors being the heat flux and the depth h, i.e. the Rayleigh flux number. For non-rotating turbulent convection Malkus (1954), Deardorff & Willis (1967) and Golitsyn (1979) obtained theoretically and confirmed experimentally the following dependence of the vertical Reynolds number on the external parameters:

$$Re_w = wh\nu^{-1} = A\,Pr^{-\frac{3}{5}}Ra_f^{\frac{1}{5}}, \tag{4.1}$$

where $A = 0.73$ according to the measurements. We have taken 167 vertical velocity measurements in the cores which agree satisfactorily with the formula (the correlation coefficient $r = 0.962$) with $A = 0.80$. We find that the vertical mean velocity of turbulent convection in the non-rotating fluid and maximal vertical velocity in the vortex cores in the rotating fluid in a regular convective regime can be described in a similar manner but with slightly different numerical coefficients. We did not have enough data to determine the aforementioned weak dependence of w on Ω.

The value of the vertical velocity is in a good accord with the lifetime of the convective rings measured in Paper 1 (see equation (3.2) there).

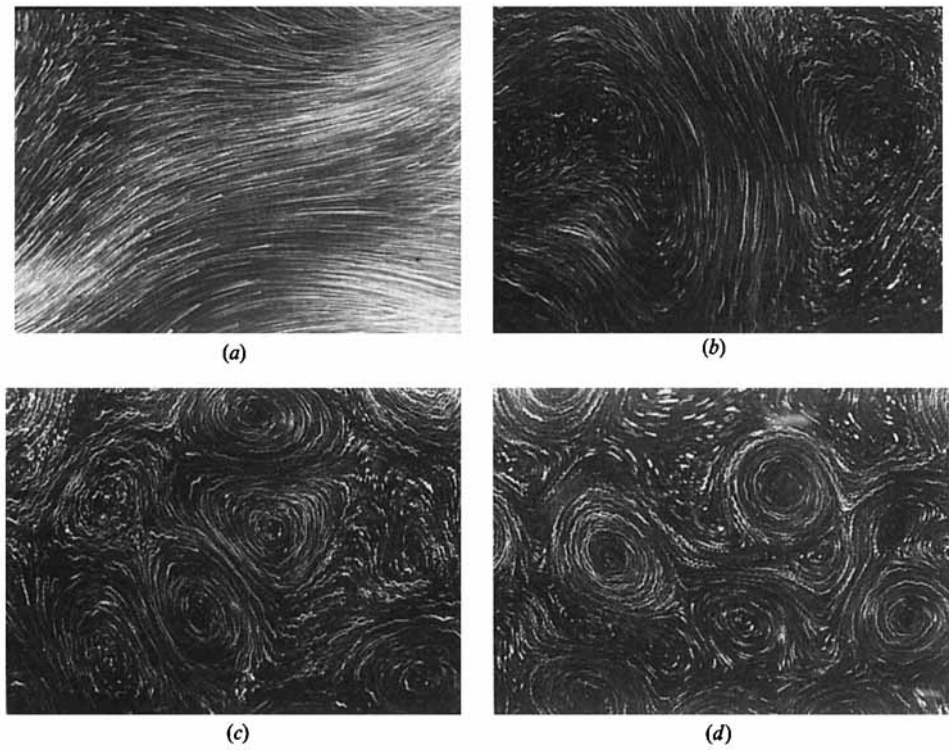

FIGURE 13. Horizontal structure of convective motions for different Ω at 2 cm from upper surface, $h = 10$ cm, $f = 150$ W m^{-2}, $Ra_f = 5.1 \times 10^8$. (*a*) $\Omega = 0$, (*b*) 0.52 s^{-1}, (*c*) 3.14 s^{-1}, (*d*) 4.19 s^{-1}.

Now we consider the horizontal velocity field in a regular vortex grid. Outside the boundary layers noticeable horizontal motions are observed only in the regions of cylinders along which the warmer fluid ascends and there is practically no horizontal motion in the vortex cores and between the cylinders (see figure 13 where vortices are somewhat irregular and interacting). Maximal horizontal velocities are observed at the cylinders of ascent and fluid particles can at any moment be transferred from one cylinder to a neighbouring one, which brings an element of randomness to the otherwise very regular structure of the vortex grid. This information was obtained by the illuminating beam technique. The same behaviour is observed by the dye visualization if the dye is injected within the fluid. In this case the dye moves not only vertically, but also horizontally between the cylinders and the horizontal velocities are comparable with the vertical ones. The radial distribution of the horizontal azimuthal velocity centred around a regular vortex is shown in figure 14 and the vertical distribution of the maximal horizontal velocity in figure 15. These two figures show that the horizontal velocity has a maximum at the cylinder, is close to zero at the vortex core and decreases sharply at the outer edge of the cylinder; the maximal velocity is near the free surface and within the main volume of fluid it slowly decreases with height, the decrease being close to linear.

4.2. *Velocities in the irregular vortex regimes*

An irregular vortex regime consists of vortices of different sizes with developed vertical jet flows at the centre of the vortex and its boundaries, the vortices moving chaotically in space and time. To determine mean horizontal velocities u the

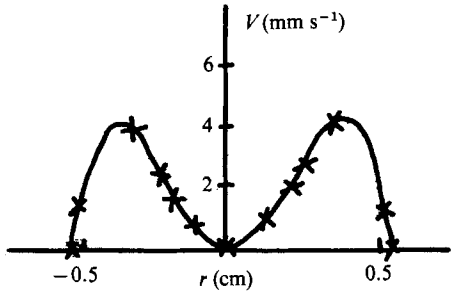

FIGURE 14. Dependence of the horizontal velocity V on the distance from the vortex centre r: $h = 10$ cm, $f = 450$ W m^{-2}, $\Omega = 4.19$ s^{-1}, $Ra_f = 2.6 \times 10^9$.

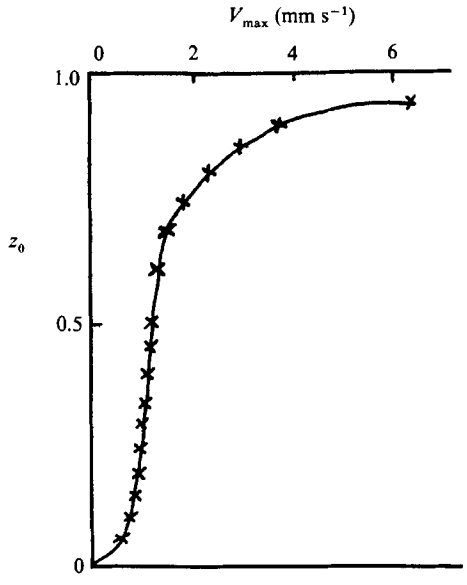

FIGURE 15. Dependence of the maximum horizontal azimuthal velocity V_{max} on z_0: $h = 20$ cm, $f = 450$ W m^{-2}, $\Omega = 4.18$ s^{-1}, $Ra_f = 4.2 \times 10^{10}$, $Ta = 2.7 \times 10^{11}$.

velocities were measured at 10 points at one level (2 cm from the surface), separated by 4 mm from each other, and the r.m.s. value was calculated and then the horizontal Reynolds number $Re_u = uh\nu^{-1}$.

We consider first mean horizontal velocities $\bar{u}$ in irregular regimes. For points in region 4 of figure 2 where the Rossby number $Ro \geqslant 1$ the value of $\bar{u}$, within the accuracy of measurements, does not depend on the rotation rate Ω. But for region 3, geostrophic turbulent convection, we have checked the dependence (2.5) which for the Reynolds number $Re = vh\nu^{-1}$ can be written as

$$Re_u = C_9 Pr^{-1} Ra_f^{\frac{1}{2}} Ta^{-\frac{1}{4}}. \tag{4.2}$$

Measurements of u by the streak photography technique were performed for $h \geqslant 10$ cm and 15 different values of Ra_f and Ta. The correlation coefficient is $r = 0.985$ between pairs of Re_u measured and calculated by (4.2). The regression coefficient $C_9 = 1.7$ which can be compared with results of a very rough experimental determination of a similar coefficient for mean vertical velocities which gave 2.3 ± 0.4

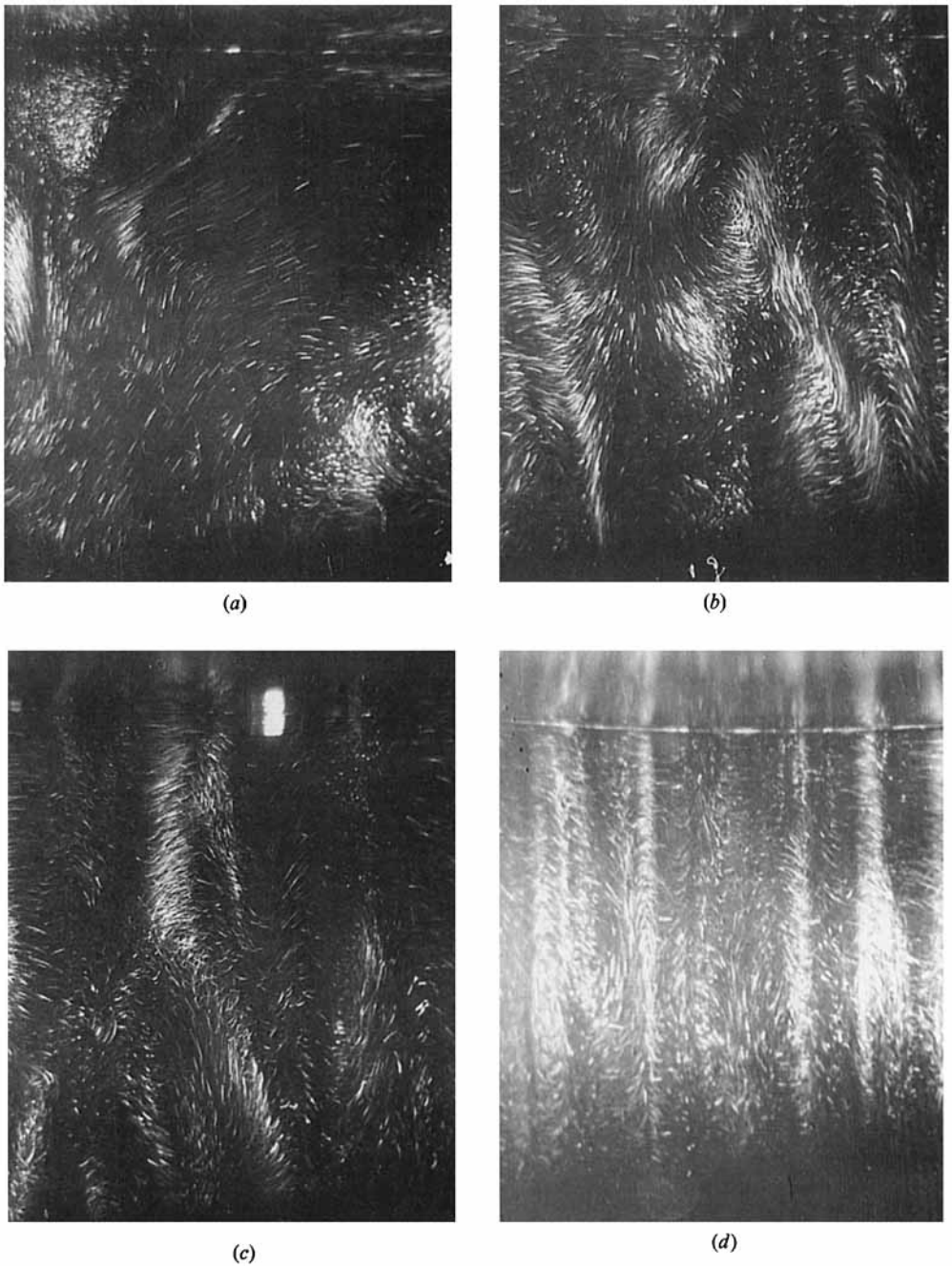

FIGURE 16. Vertical structure of convective motions for $h = 10$ cm, $f = 450$ W m^{-2}, $Ra_f = 2.6 \times 10^9$ and different values of Ω: (*a*) $\Omega = 0$, (*b*) 0.52 s^{-1}; (*c*) 2.09 s^{-1}; (*d*) 4.19 s^{-1}. At the upper parts of the photographs one can see the reflections from the fluid upper surface.

(Golitsyn 1981). Similar measurements were recently made by Fernando, Boyer & Chen (1989). They also confirmed (4.3) with $C_9 = 1.6$.

The visualization by the aluminium powder allows one to clearly see the character of motions within the system. Figure 13 shows the evolution of the motion patterns

with a sequential increase of the rotation rate Ω. From global motions comparable with the vessel size at $\Omega = 0$ the system acquires the structure of local vortices as described in Paper 1. In turbulent regimes the vortices are large and the motion between them is seen clearly. At higher rotation rates the vortices get smaller and more localized, stagnation points are seen and the motion of particles between the cylinders is much weaker.

Figure 16 presents streak photographs of vertical cross-sections by the light beam of our vessel with increasing rotation Ω. At $\Omega = 0$ we see a flow comparable in size with the vessel. The structure becomes more localized with the increase of Ω. At small Ω the orientation of the vortex axes is rather arbitrary in space; at larger Ω the vortices tend to align along the rotation axes and at sufficiently large Ω all vortices are of the same sign and direction as Ω.

5. Discussion and conclusions

The study reported has shown the richness of phenomena observed in fairly simple, at least at first sight, experiments. Most researchers have concentrated on the initial stages of convection development which is easier from theoretical point of view and without which it would be difficult to understand many effects. But the regimes of developed convection with rotation remained virtually unexamined. At moderately large supercritical Rayleigh numbers but not large Taylor numbers the rotation influences the convection structure little and the fluid motion 'remembers' its structure at $\Omega = 0$. Also, the processes in the boundary layers are of much significance and at smaller Taylor numbers the motion in these layers determines fully the fluid layer motions.

For developed convection the fluid outside the boundary layers has a practically homogeneous (with respect to certain statistical properties) region. In the regular regime the convection is characterized by the following features.

(i) The ascent of the fluid occurs on cylinders while its sinking is confined to an intense jet (vortex core) at the cylinder axis. Inside the cylinder the fluid particles move along fixed trajectories which at the cylinder surface or between the cylinders the motion is rather irregular and a fluid particle can at any moment leave the surface or go from one surface to another neighbouring one. After Chandrasekhar (1961) and Veronis (1959) there is a notion that the motion in a convective rotating layer is on conical surfaces with a change of the rotation sign in a vortex when a fluid particle moves down from the surface to the bottom. In our experiments we sometimes observed cone-like shapes only at the beginning of the regime development in the parameter space close to the critical curve, but with time the cones transformed into cylinders and their rotation sign was always that of the basic rotation of the system. Evidently the cones are unstable configurations. In this respect the work by Goncharov & Gryanik (1986) may have some relevance. They considered the grid of Sallivan vortices with flow patterns close to what we observed and they proved that such a rotating vortex grid is stable.

(ii) The fact that a fluid particle can spontaneously go from one cylindrical surface to another one does not allow us to say that the regular regimes (in our terminology) are regular in any rigorous sense. On the one hand, we have a stable vortex structure with fixed vortices forming a regular grid. On the other hand, we have full indeterminacy of individual fluid particle trajectories on cylinder surfaces.

(iii) The temperature gradient within the main part of a layer with a regular vortex grid is constant, i.e. the temperature profiles are linear with height. The

gradient values are functions of Ω, fluid depth and Rayleigh flux number, which results in a heat transfer relationship $Nu \propto Ra^3 Ta^{-2}$. This relationship leads to the independence of the heat flux through the layer of its height and may be confirmed by some indirect experimentally based arguments. It was also suggested by some earlier theoretical work.

Irregular vortex regimes, in their turn, can be divided into two regimes, geostrophic convection and thermal convection.

(iv) In both of these regions the temperature in the main body of fluid outside the boundary layers does not change with height. There is a universal temperature power spectrum in non-dimensional coordinates that is similar for both regions, except that the timescale in the region of geostrophic convection is about three times larger than for the usual thermal convection. The intensity of the spectra in the geostrophic region is directly proportional to the rotation rate Ω and the heat flux.

(v) New experiments confirm much cruder older ones in establishing the velocity scale for geostrophic convection $\bar{u} \approx 2(\epsilon/2\Omega)^{\frac{1}{2}}$ derived previously by dimensional arguments, with ϵ being the kinetic energy dissipation and 2Ω the Coriolis parameter.

Though arguments may be developed that for geostrophic convection the heat transfer can obey the same relationship $Nu \propto Ra^3 Ta^{-2}$, or a similar one, for very large values of the Rayleigh and Taylor numbers this problem awaits systematic experimental studies.

It can be shown that geophysical applications of geostrophic convection are motions within the Earth's liquid core, deep convection in the ocean (Golitsyn 1980, 1981) and in basaltic magma chambers (Griffiths 1987). For the first case, assuming a geothermal heat flux of the same order as on the surface (or less), we can obtain $\bar{u}$ of the order of few kilometres per year which corresponds to the drift rate of certain geomagnetic field components. For the latter case with $f = 1$–10 W m^{-2} the velocity scale would be of order of 1 or few mm/s, i.e. 30 or more km/year. A detailed discussion of geophysical applications will be presented elsewhere.

The authors are grateful to V. N. Ivanov, A. O. Senatorsky and V. A. Filatov who helped us in doing some calculations and measurements. We also thank three referees whose questions and comments helped for a more concise and clear presentation of the material.

REFERENCES

BOUBNOV, B. M. 1987 Thermal structure of vortex convective grid. *Izv. Akad. Nauk. SSSR Mech. Zhid. i Gaza* **6**, 160–166.

BOUBNOV, B. M. & GOLITSYN, G. S. 1986 Experimental study of convective structures in rotating fluids. *J. Fluid Mech.* **167**, 503–531 (referred to as Paper 1).

BOUBNOV, B. M. & SENATORSKY, A. O. 1988 Influence of boundary conditions on convective stability of horizontal rotating fluid layer. *Izv. Akad. Nauk. SSSR Mech. Zhid. i Gaza* **3**, 124–129.

BUSSE, F. H. & HIKES, K. E. 1980 Convection a rotating layer: A simple case of turbulence. *Science* **208**, 173–174.

CHAN, S. K. 1974 Investigation of turbulent convection under a rotation constraint. *J. Fluid Mech.* **64**, 477–506.

CHANDRASEKHAR, S. 1953 The instability of a layer of fluid heated below and subject to Coriolis forces. *Proc. R. Soc. Lond.* A **217**, 306–327.

CHANDRASEKHAR, S. 1961 *Hydrodynamic and Hydromagnetic Stability*. Clarendon.

CORRSIN, S. 1951 On the spectrum of temperature fluctuations in an isotropic turbulence. *J. Aeronaut. Sci.* **22**, 469–473.

DEARDORFF, J. W. 1970 Convective velocities and temperature scales for the unstable boundary layer and for Rayleigh convection. *J. Atmos. Sci.* **27**, 1211–1213.

DEARDORFF, J. W. & WILLIS, G. E. 1967 Investigation of turbulent thermal convection between horizontal plates. *J. Fluid Mech.* **28**, 675–705.

FERNANDO, H. J. S., BOYER, D. L. & CHEN, R. 1989 Turbulent thermal convection in rotating fluid. *Euromech 245, Cambridge, April 1989.*

FITZJARRALD, D. E. 1976 An experimental study of turbulent convection in air. *J. Fluid Mech.* **73**, 693–721.

FOSTER, T. D. 1969 The effect of initial conditions and lateral boundaries on convection. *J. Fluid Mech.* **37**, 81–95.

FOSTER, T. D. & WALLER, S. 1985 Experiments on convection at very high Rayleigh numbers. *Phys. Fluids* **28**, 455–461.

GINSBURG, A. J., GOLITSYN, G. S. & FEDOROV, K. N. 1979 Measurements of time scale of convection in fluid during cooling from the surface. *Izv. Atmos. Oceanic Phys.* **15**, 333–335.

GOLITSYN, G. S. 1979 Simple theoretical and experimental study of convection with some geophysical applications and analogies. *J. Fluid Mech.* **95**, 567–608.

GOLITSYN, G. S. 1980 Geostrophic convection. *Dokl. Acad. Nauk SSSR* **251**, 1356–1360.

GOLITSYN, G. S. 1981 Structure of convection at fast rotation. *Dokl. Acad. Nauk SSSR* **261**, 217–320.

GONCHAROV, V. P. & GRYANIK, V. M. 1986 Dynamics of solitary dissipative vortices: vortex lattices and their stability. *Sov. Phys. J. Exp. Theor. Phys.* **64**, 976–983.

GRIFFITHS, R. M. 1987 Effects of Earth's rotation on convection in magma chambers. *Earth and Planet. Sci. Lett.* **85**, 525–536.

GURVICH, A. S. & YURCHENKO, B. N. 1980 Frequency spectra of the temperature fluctuations in the turbulent convection. *Izv. Atmos. Oceanic Phys.* **16**, 854–857.

HOWARD, L. N. 1963 Heat transport by turbulent convection. *J. Fluid Mech.* **17**, 405–432.

KATSAROS, K. B., LIU, W. T., BUSINGER, J. E. & TILLMAN, J. E. 1977 Heat transport and thermal structure in the interfacial boundary layer measured in an open tank of water in turbulent free convection. *J. Fluid Mech.* **83**, 311–335.

KIRDYASHKIN, A. G. & SEMENOV, V. J. 1983 Temperature fluctuation spectra in vertical layer in thermal gravitational convection. *Thermophys. High Temperature* **21**, 731–739.

MALKUS, V. V. R. 1954 The heat transport and spectrum of thermal turbulence. *Proc. R. Soc. Lond.* A **225**, 196–212.

NAKAGAWA, Y. & FRENZEN, P. 1955 A theoretical and experimental study of cellular convection in rotating fluids. *Tellus* **7**, 1–21.

OBOUKHOV, A. M. 1949 The structure of temperature field in turbulent flow. *Izv. Akad. Nauk. SSSR Geogr. Geophys.* **13**, 58–69 (in Russian).

OBOUKHOV, A. M. 1960 On structure of temperature field and field of velocities in condition of free convection. *Izv. Akad. Nauk. SSSR Geophys.* **9**, 1392–1396 (in Russian).

PRANDTL, L. 1932 Meteorologische Anwendungen der Stromungslchere. *Beitr. Z. Phys. Atmos.* **19**, 188–202.

RIAHI, N. 1977 Upper-bound problem for a rotating system. *J. Fluid Mech.* **81**, 523–526.

ROSSBY, H. T. 1969 A study of Bénard convection with and without rotation. *J. Fluid Mech.* **36**. 309–337.

VERONIS, G. 1959 Cellular convection with finite amplitude in rotating fluid. *J. Fluid Mech.* **24**. 545–554.

ZIMIN, V. D. & KETOV, A. I. 1978 Turbulent convection in a cubic cavity heated from below. *Izv. Akad. Nauk. SSSR Mech. Zhid. i Gaza* **4**, 133–138.